Sheffield Hallam University

Heat transfer performance of compact TPMS lattice heat sinks via metal additive manufacturing

CHOUHAN, Ganesh, NAMDEO, Avinash Kumar, GUNER, Ahmet, ESSA, Khamis and BIDARE, Prveen

Available from Sheffield Hallam University Research Archive (SHURA) at:

https://shura.shu.ac.uk/36208/

This document is the Published Version [VoR]

Citation:

CHOUHAN, Ganesh, NAMDEO, Avinash Kumar, GUNER, Ahmet, ESSA, Khamis and BIDARE, Prveen (2025). Heat transfer performance of compact TPMS lattice heat sinks via metal additive manufacturing. Progress in Additive Manufacturing. [Article]

Copyright and re-use policy

See http://shura.shu.ac.uk/information.html

Sheffield Hallam University Research Archive
http://shura.shu.ac.uk

Progress in Additive Manufacturing
https://doi.org/10.1007/s40964-025-01366-0

RESEARCH

Heat transfer performance of compact TPMS lattice heat sinks via metal additive manufacturing

Ganesh Chouhan[1] · Avinash Kumar Namdeo[2] · Ahmet Guner[3] · Khamis Essa[4] · Prveen Bidare[5]

Received: 9 July 2025 / Accepted: 16 September 2025
© The Author(s) 2025

Abstract

Nature-inspired triply periodic minimal surface (TPMS) lattices serve as exemplary models for advanced thermal management strategies. Their intricate geometric and topological configurations enhance surface area, porosity, and smooth curved walls, optimizing thermal performance across diverse applications. These attributes render TPMS structures exceptionally effective in augmenting heat sink performance within a constrained volume, outperforming conventional designs such as pin fin heat sinks. The present study evaluates the thermal performance of five L-PBF manufactured TPMS heat sinks (Gyroid, Diamond, Schwarz, Lidinoid, and Split P) relative to conventional pin–fin heat sinks of equivalent volume. The investigation focuses on the effect of unit cell sizes and periodicity on thermal performance, providing deeper insights into heat transfer mechanisms in TPMS-based structures. To accurately replicate the thermal characteristics, both numerical simulations and experimental testing were conducted. A customized testing system was developed to assess A20X aluminum heat sinks, revealing uniform heat flow across the lattice samples. Overall, this study indicates potential for improved heat transfer and validates the superior performance of TPMS heat sinks over traditional designs.

Keywords Compact heat sink · Triply periodic minimal surface · Laser powder bed fusion · Additive manufacturing · Surface area · Heat transfer

1 Introduction

Electronics and mechanical industries are frequently adopting compact and ultra-light designs to attract customers. Currently, the failure frequency of digital components rises for compact design [1–4]. The compact design generates more heat, demanding the development of a device with a larger surface area to increase the heat transfer rate and maintain the compact and lightweight structure. Conventional thermal management (i.e., heat sinks) is not sufficient to fulfill the present demand [5]. Industries that rely on thermal instruments extensively optimize the internal parameters of heat transfer devices, including the augmentation of surface area, to enhance thermal contact between surfaces and heat.

Triply periodic minimal surfaces (TPMS) represent a class of implicit designs characterized by three-dimensional smooth surfaces, renowned for their ability to minimize localized regions. Considering a mean curvature of zero, these surfaces separate space into two intricately woven domains where the sum of the curvatures at each point on the surface is zero [6] and under specific boundary conditions,

✉ Ganesh Chouhan
ganesh.chouhan@medicaps.ac.in

✉ Prveen Bidare
p.bidare@shu.ac.uk

Avinash Kumar Namdeo
dr.avinashkumarnamdeo@gmail.com

Ahmet Guner
ahmet_guner@hotmail.com

Khamis Essa
k.e.a.essa@bham.ac.uk

[1] Department of Mechanical Engineering, Medi-Caps University, Indore, India

[2] Lingaya's Vidyapeeth, Faridabad, India

[3] School of Metallurgy and Materials, University of Birmingham, Birmingham, UK

[4] School of Mechanical Engineering, University of Birmingham, Birmingham, UK

[5] School of Engineering and Built Environment, University of Sheffield, Sheffield, UK

Published online: 30 September 2025

the TPMS area is limited. Furthermore, these surfaces exhibit a tendency to maintain their lowest energy state in natural systems. Consequently, TPMS lattices are frequently observed, as any increase in surface area necessitates additional surface energy, reinforcing their prevalence in various natural contexts. These lattice structures are characterized by several key features, including bioinspiration from natural examples such as butterfly wings, weevils, the human retina, and beetle shells; long-range order, which results in lightweight designs with high strength and increased surface area; and a mathematical definition based on implicit equations [7]. The thermal performance of TPMS structures can be systematically optimized through the precise adjustment of key parameters, including porosity, unit cell morphology, unit cell dimensions, and the overall structural topology. This flexibility makes it possible to modify thermal conductivity to satisfy the unique needs of multiple uses [8]. TPMSs are currently utilized in shape optimized [9], composite materials [10], and heat transfer [11] due to their diverse patterns. However, conventional subtractive machining faces significant challenges due to the complex and tortuous geometry of these structures. Consequently, additive manufacturing (AM) emerges as a necessary technique for the fabrication of TPMS [12].

The triply periodic minimal surface lattice heat sinks achieved better heat transfer results [13–15] in free and forced conditions. The performance of TPMS heat sinks can be improved by optimizing the parameters, such as unit cell size, cylindrical coordinates, and cylindrical different design parameters. Numerous studies have concentrated on various heat sink designs, such as corrugated channels [16], reduced fins [17], mini channels [18], microchannels [19], honeycomb, radially curved, flared [20], rectangular and triangular perforation [21], Simple Cubic, Voronoi, tpms metal foam [22], and Octet lattice heat sinks [23] for heat management tasks. Researchers continuously modify multiple control variables to optimize lattice structures for enhanced heat dissipation performance in specific applications. Benjamin Vaissier et al. [24] considered parameters like design space definition, lattice selection and orientation, wireframe generation, lattice volume grading and meshing, and unification for improvement of heat sink performance. Ramendra Singh Niranjan et al. [25] designed and experimented with micropin fins heat sinks of varying heights and spacings, and noticed that the cooling efficacy was 10% greater than that of conventional plate fin sinks. Abhijeet Gaikwad et al. [26] presented an extensive review of fin heat sinks which addressed heat transfer improvement methods, an examination of various fin designs, and the application to current electronic devices. The lattice structure has been developed using various additive manufacturing methods, including stereolithography [27], extrusion-based [28], LPBF [12], binder jetting [29], and EBM [30].

Modern manufacturing, particularly the energy transfer industry (i.e., heat sinks, heat exchangers, heat pipes), increasingly relies on additive manufacturing to produce tailored organic shapes that outperform conventional ones [31, 32]. The most potential additive manufacturing method for precision industrial applications is the powder bed fusion process. The LPBF method creates a component by selectively fusing material provided as a fine powder inside a powder bed [33]. This method of fabricating a complex geometry in a single body could present several benefits over traditional manufacturing approaches, involving a reduction in the overall number of elements, a greater output rate, and fewer geometric restraints [34]. Numerous materials have been explored to refined the thermal performance of heat sinks, with notable examples, including phase change material [35], and copper and aluminum [36] (Fig. 1).

Aluminum exhibits exceptional thermal conductivity, which facilitated its utilization in the additive manufacturing printing of intricate, monolithic heat sinks for lighting applications. A20X is an efficient aluminum alloy developed especially for applications, including strength, lightweight, and superior corrosion resistance. This alloy is remarkable for being used in the automotive and aerospace sectors, where structural integrity is maintained, while weight reduction is essential [37]. The precipitation-hardening alloy A20X (Al–Cu–Ag–Mg–TiB2) was created recently for use in additive manufacturing [38]. Its unique composition improves its mechanical characteristics, including as fatigue resistance and yield strength. The alloy is appropriate for applications in which heat dissipation is crucial due to its notable thermal conductivity. This innovative approach not only enhances efficiency but also transforms the way we manage heat in lighting technology. Additionally, it is characterized by its ease of forming and moderate machinability, though it is less machinable than free-machining alloys.

This study heralds a transformative leap in the realm of compact heat sink design and production. Leveraging the innovative potential of TPMS lattice structures, characterized by dual unit cell sizes and varying periodicity, enables the exploration of new frontiers in thermal performance enhancement. This research not only advances thermal simulation and experimental testing but also redefines the parameters for LPBF printed heat sinks, setting a new standard for efficiency and effectiveness in thermal management.

This study explores the development of bio-inspired heat sink designs to improve thermal dissipation by leveraging biomimetic principles. The TPMS proposed designs (Diamond, Gyroid, Split P, Schwarz, and Lidinoid) aim to enhance thermal conduction from electronic components while reducing the overall size of the heat sink, without compromising thermal efficiency. Each lattice was designed with 5 mm and 10 mm unit cells in nTopology and fabricated via LPBF. This study aims to analyze thermal performance

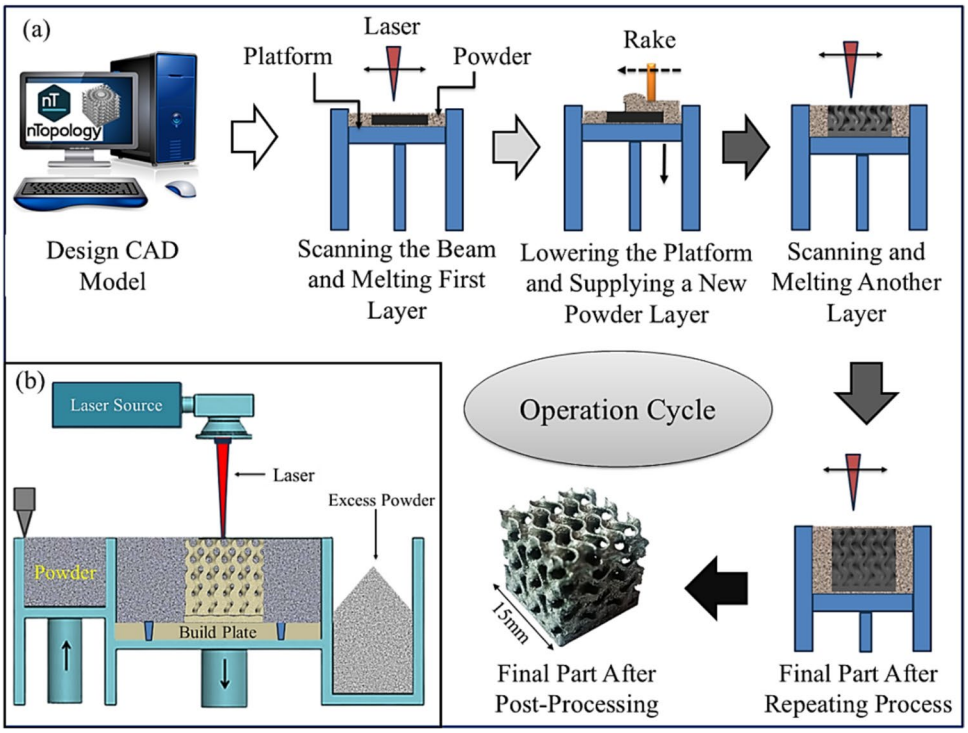

Fig. 1 Schematic illustration of **a** process cycle for LPBF and **b** the experimental apparatus setup

by examining the effects of unit cell size and periodicity through thermal simulations and experimental testing on a customized system. The findings contribute to a more comprehensive understanding of heat transfer mechanisms in TPMS-based architectures.

2 Material and methodology

2.1 TPMS heat sinks designs

This section explores how level-set approximation equations shape the design and fabrication of five TPMS-based heat sinks, as detailed in Table 1. TPMS lattices excel in heat transfer by maximizing the surface-area-to-volume ratio and being inherently self-supporting, omitting extra structures. This approach lowers manufacturing costs while eliminating the need to remove internal supports, a challenging and often impractical task in complex geometries that could compromise the lattice structure's integrity.

Fourteen lattice heat sinks were designed using nTopology and printed via LPBF with A20X aluminum alloy. Five TPMS-based lattices feature standard periodicity, while gyroid and diamond variants have varying periodicities for comparison. Each lattice structure comes in two variations, both with a consistent 2 mm base and 1 mm strut thickness. Gyroid and diamond lattice configurations were employed to develop two cylindrical designs with varying periodicities. To facilitate a rigorous comparative analysis of these geometries, a fixed volumetric constraint of $15 \times 15 \times 15$ mm^3 and unit cell sizes 5 and 10 mm was imposed.

Figure 2 displays the different selected TPMS surfaces with different unit cell (UC) and cylindrical unit cell (CSUC).

2.2 Surface area measurement and comparisons

In this study, nTopology software was utilized to define this volume and facilitate the generative design of a heat sink, with the objective of maximizing surface area while minimizing mass. As shown in Table 2, a larger surface area has been computed for the split P (5), Lidinoid (5), and Diamond (CS-5) lattice heat sinks. In contrast to standard periodicity diamond heat sink, the surface area of the unit cell sizes 5 and 10 of the variable periodicity diamond heat sinks is 9.8% and 33% larger, respectively. A comparative analysis of the surface area between conventional and TPMS lattice heat sinks revealed that TPMS lattice heat sinks exhibit twice the surface area of their conventional counterparts.

2.3 Additive manufacturing of selected designs

In this section, 14 TPMS heat sink designs were translated from digital models to physical prototypes. The CAD models were systematically converted into STL files, followed by the generation of slice data necessary for integration with the additive manufacturing system. Lattice samples were

Table 1 TPMS lattice implicit surface modeling equations

Surfaces	Implicit surface modeling equations $\Phi(x, y, z) = t$
Diamond	$\sin(\omega x)\sin(\omega y)\sin(\omega z) + \sin(\omega x)\cos(\omega y)\cos(\omega z) + \cos(\omega x)\cos(\omega y)\sin(\omega z)$
Gyroid	$\sin(\omega x)\cos(\omega y) + \sin(\omega y)\cos(\omega z) + \sin(\omega z)\cos(\omega x)$
Lidinoid	$\sin2(\omega x)\cos(\omega y)\sin(\omega z) + \sin2(\omega y)\cos(\omega z)\sin(\omega x) + \sin2(\omega z)\cos(\omega x)\sin(\omega y) - \cos2(\omega x)\cos2(\omega y) - \cos2(\omega y)\cos2(\omega z) - \cos2(\omega z)\cos2(\omega x) + 0.3$
Schwarz P	$\cos(\omega x) + \cos(\omega y) + \cos(\omega z)$
Split P	$1.1(\sin2(\omega x)\sin(\omega z)\cos(\omega y) + \sin2(\omega y)\sin(\omega x)\cos(\omega z) + \sin2(\omega z)\sin(\omega y)\cos(\omega x)) - 0.2(\cos2(\omega x)\cos2(\omega y) + \cos2(\omega y)\cos2(\omega z) + \cos2(\omega z)\cos2(\omega x)) - 0.4(\cos2(\omega x) + \cos2(\omega y) + \cos2(\omega z))$

$\omega x = X$, $\omega y = Y$, $\omega z = Z$ are the functional periodicity of TPMS lattice, and ω represents functional periodicities of the TPMS lattice which relates the periodicity for unit cell length. $\omega = \frac{2\pi}{l_i}$, and l_i represents the unit cell length

produced at the University of Birmingham using the Concept Laser M2 system, equipped with a 200 W fiber laser, a 250×250 mm^2 work area, 150 µm focal diameter, and scanning speeds of up to 7000 mm/s. The chamber atmosphere was composed of argon and maintained at an oxygen content below 0.1% and slice thickness of 20 µm to ensure optimal conditions for sample fabrication.

The optimal material for TPMS heat sinks should exhibit high thermal conductivity, mechanical strength for thin walls, and compatibility with complex geometries. Al–Cu alloys doped with TiB_2 effectively satisfy these criteria. The TPMS heat sinks were fabricated using gas-atomized A20X aluminum powder, spherical, featuring a mean grain size of 40 µm and a grain size distribution between 20 and 60 µm. To balance mechanical performance and lightweight qualities, A20X, a strong aluminum alloy reinforced with titanium diboride (TiB_2), has a low density, high coefficient of thermal expansion, and an ultimate tensile strength of about 475 MPa. The principal characteristics and chemical specification of A20X have been presented in Fig. 3. The generated TPMS lattice structures accurately followed the design criteria, with interconnected unit cells and consistent geometry.

The main features of additive manufacturing and laser specifications are presented in Fig. 4 using lateral surface measurements of vertically constructed lattice samples (Fig. 5).

2.4 Experimental apparatus and test procedure

A custom test rig was built to validate numerical results. Figure 6 illustrates the experimental setup for analyzing thermal performance of LPBF lattice heat sinks. The test setup comprised a DC power supply (WANPTEK-CHAAL-AKAM SMPS, 0–30 V, 0–5 A, 150 W; Middle Shennan Road, Shenzhen, China), an XH-W1219 12 V digital temperature controller module, a band heater, heat sink samples, data acquisition system (Keysight 34980A; Santa Rosa, CA, USA), and computer. A 20 mm in diameter and 50 mm in height copper cylinder block is integrated with a ring band heater constructed from 304 stainless steel. This heating assembly is rated at 980 watts and incorporates mica insulation alongside a Nichrome 80/20 wire for electric heating. This configuration facilitates efficient heat transfer and uniform temperature distribution, critical for various thermal applications. An almost uniform temperature distribution was created at the heat sink-copper block contact (size ϕ20 mm and height 50 mm), attributed to the high thermal conductivity of copper. The band heater was securely fastened to the copper rod to ensure optimal thermal conductivity. The temperature variation across this interface was minimal, with a difference of only 0.5 °C. Glass fiber is utilized as the insulating material and encloses the

heater, test specimen, copper block, and metal chamber to reduce heat losses. A heat sink is strategically positioned in the upper section of the copper bar, utilizing a thermal paste to facilitate optimal thermal conductivity. This application of thermal paste enhances the interface between the heat sink and the copper substrate, thereby improving heat transfer efficiency. Such configuration is critical in ensuring effective thermal management within the system, ultimately contributing to enhanced performance and reliability. The test samples were positioned within the testing area, situated atop a copper block that was enveloped by a band heater. For all sample tests, the test section remained fixed in position,

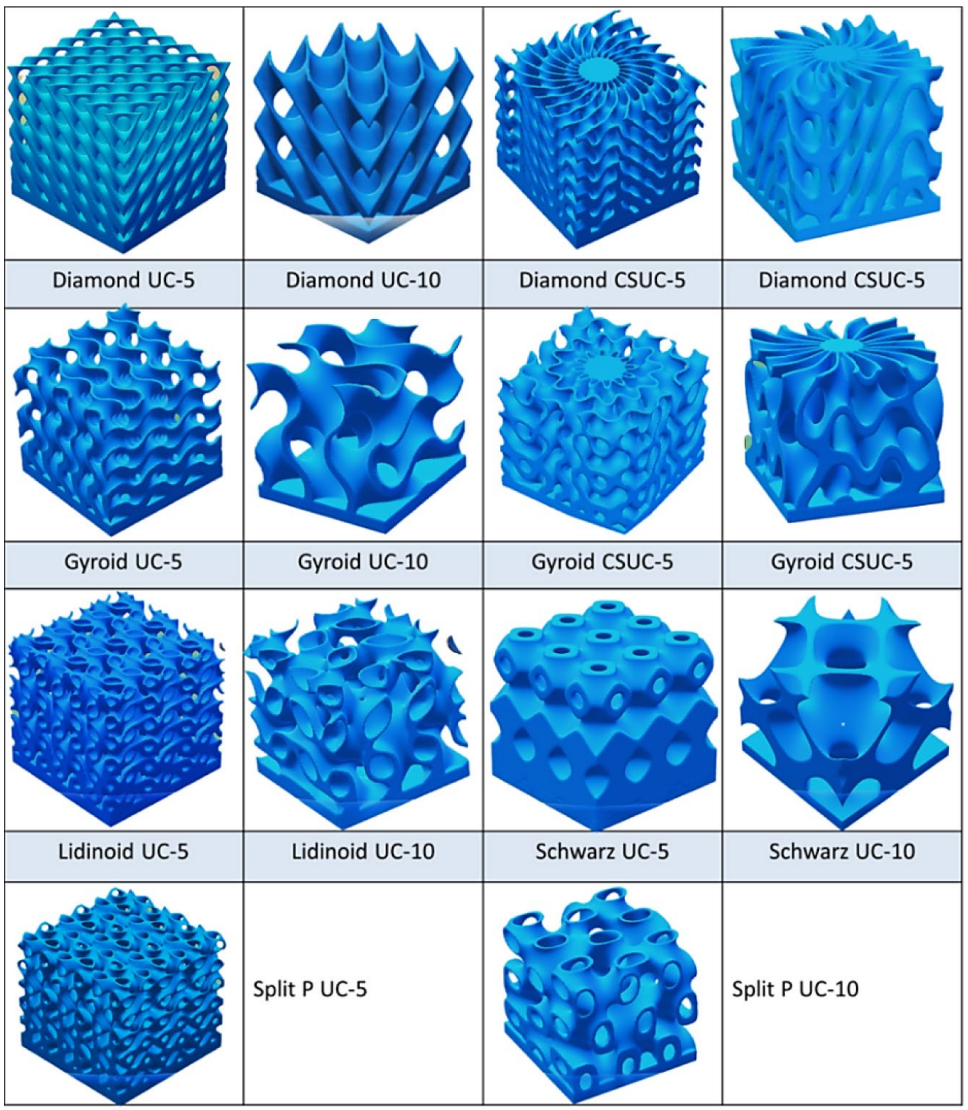

Fig. 2 Advanced TPMS-inspired compact heat sinks demonstrating unit cell scaling and periodicity variation

Table 2 Structures, sizes and measured surface area of the TPMS samples

Lattices	Unit cell size	Surface area (mm^2)	Lattices	Unit cell size	Surface area (mm^2)
Diamond	5	4687.45	Gyroid	5	4069.36
Diamond	10	2821.62	Gyroid	10	2395.97
Diamond	5	5196.06	Gyroid	5	4771.36
Diamond	10	4200.04	Gyroid	10	3625.56
Lidinoid	5	5637.60	Schwarz	5	2756.60
Lidinoid	10	3789.56	Schwarz	10	1981.97
Split P	5	5698.24	Conventional pin fin	5×5	2344.94
Split P	10	3620.98			

ensuring uniformity and precision throughout the experimental procedure.

The Arduino M152 is a digital thermostat temperature control switch operating at 12 V, featuring a temperature-controlled relay with a high control accuracy of 0.1 °C which has been utilized for measuring temperature on heat sinks. It provides a temperature control range from − 20 to 110 °C. The resolution reaches − 9.9 to 99.9 when the temperature is at 0.1 °C. The sensor dimensions are approximately 67 × 42 × 18 mm. This device functions within environmental conditions of − 10 °C to 60 °C, with a relative humidity range of 20–85%. Power consumption is efficient, with a quiescent current of ≤ 10 mA and an operating current of ≤ 65 mA. An integrated MCU chip enhances intelligent control capabilities, allowing the sensor to enforce safety measures by automatically opening the relay if temperature measurements exceed the specified range.

Pre-calibrated, high-precision NTC temperature sensors were positioned at various locations on the heat sink to monitor temperature values during the powering and draining phases of the heater at 60 s interval. The accuracy was validated across a temperature range of 35–105 °C. To obtain accurate temperature readings, two thermocouples, designated N1 and N2, were placed on the higher and lower faces of the heat sink. A DC power source was utilized to supply input power levels of 10 W, 20 W, and 30 W to the heater, enabling the evaluation of the heat generation rate. A data logger was utilized to accurately record thermocouple temperature measurements.

2.5 Assumptions and governing equations

In this study, the following assumptions were made to model steady-state conduction:

- Steady-state conduction is considered applicable.
- The materials in the model are assumed to be homogeneous, isotropic, and temperature-independent.
- Thermal conductivity is presumed to be independent of temperature variations.
- Heat generation is negligible, and heat transfer by radiation is not considered.

Under steady-state conditions, all heat transferred from the base of the heat sinks to the top is dissipated into the environment through convection. The experimental heat transfer coefficient of the fins can be found by combining Fourier's law of heat conduction and Newton's law of cooling.

Total heat at area A:

$$q_{\text{conduction}} = KA\frac{\mathrm{d}T}{\mathrm{d}x}. \tag{1}$$

Total heat rate (over surface area A):

$$q_{\text{convection}} = hA\left(T_s - T_\infty\right). \tag{2}$$

A is the actual external surface area of the specific lattice heat sink.

The surface area utilized in this equation is adjusted based on the specific lattice heat sink under investigation.

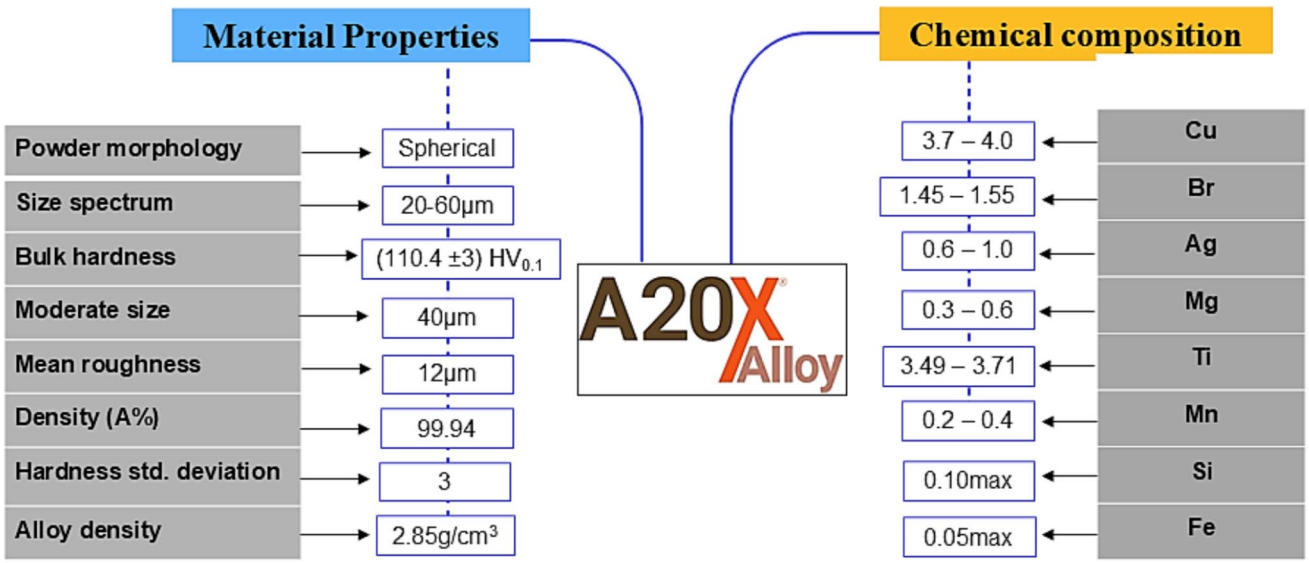

Fig. 3 Characterization and chemical composition of A20X aluminum alloy [12]

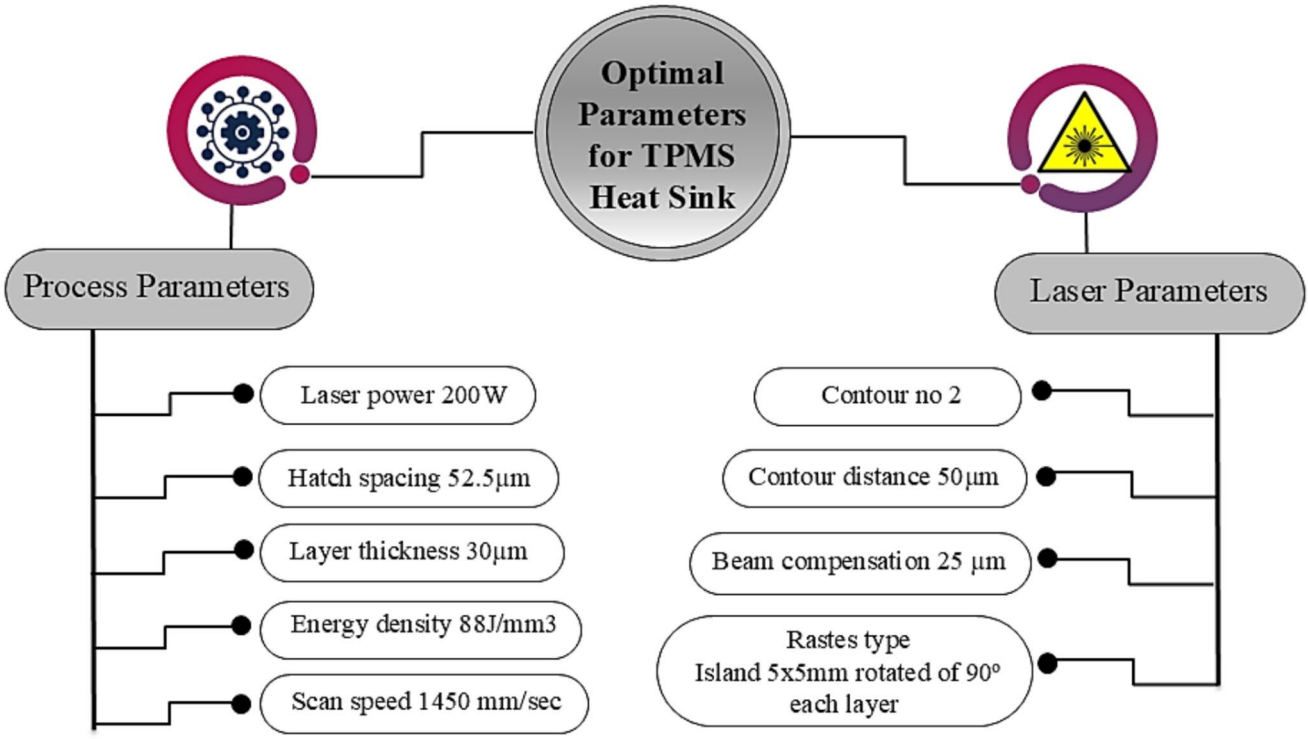

Fig. 4 Optimized LPBF process variables for A20X heat sinks

Heat conduction within the system is governed by the subsequent partial differential equation, which characterizes the three-dimensional temperature distribution

$$\frac{\partial^2 T}{\partial x^2}k_x + \frac{\partial^2 T}{\partial y^2}k_y + \frac{\partial^2 T}{\partial z^2}k_z + Q = 0, \tag{3}$$

where

- T is the pattern of temperature as an indicator of system location.
- Q represents the internal heat generation rate from the band heater.
- K_x, K_y, and K_z represents thermal conductivities along the x-, y-, and z-axes, respectively.
- Bottom face temperature: 473 K
- Radiation parameters for fins: 293 K and 0.3 emissivity
- Convection parameters for fins: 293 K and convection heat transfer coefficient 20 W/m^2 K.

3 Results and discussion

Based on the temperature distribution observed across all heat sinks, as illustrated in Figs. 6, 7, 8 and 9, the results of the analysis conducted using a fine mesh of the samples. The analysis reveals both the maximum and minimum temperatures of the heat sinks. It can be concluded that adequate temperature gradients are present within the TPMS internals, facilitating significant heat transfer between the heat source and the sample. A larger temperature gradient between the maximum and minimum values indicates a higher rate of heat transfer, as heat naturally flows from regions of higher to lower temperatures. All TPMS heat sinks exhibit uniform heat distribution across the entire structure, ensuring consistent thermal performance. In contrast, conventional pin–fin heat sinks display a non-uniform heat flow pattern. Specifically, the right corner pins demonstrate reduced thermal activity, while the left corner pins exhibit significantly higher heat accumulation, as indicated by localized hotspots.

In Fig. 7, elevated temperature regions are evident near the lower portion of the diamond lattice sink, while no comparable features are observed in the upper sections. In the middle to upper plane, a distinct, bright thermal boundary layer (indicated by yellow and green zones) is present; thinner boundary layers, as observed here, can enhance heat transfer performance. However, the prevailing temperature range in the second plane remains moderate, between 96 and 98 °C.

As anticipated, a consistent trend was observed in Fig. 8, the gyroid heat sink exhibits a more uniform temperature distribution, with peak temperatures reaching 103.58 °C but dissipating more evenly throughout the structure. This

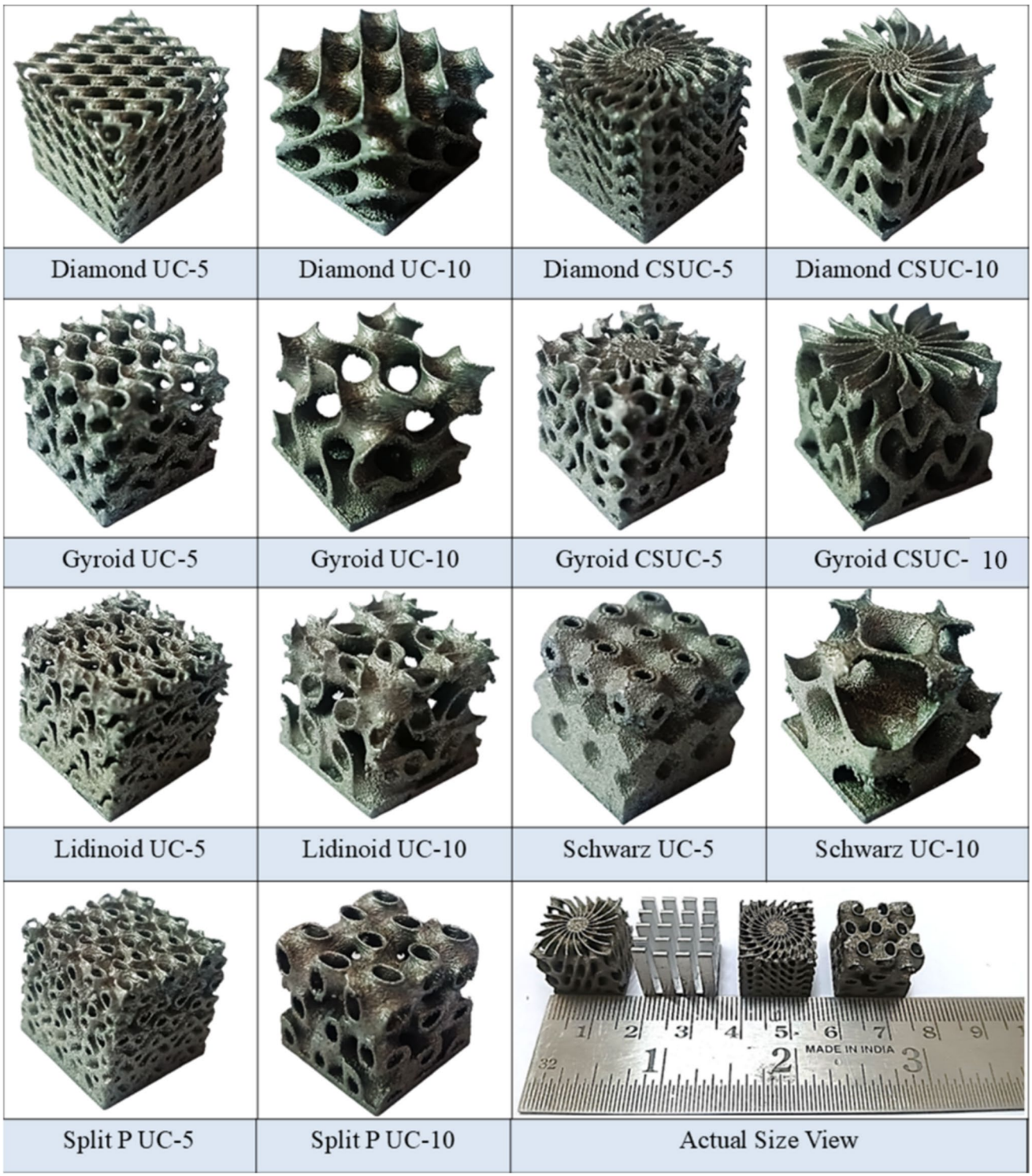

Fig. 5 A20X metal lattice heat sinks with varying unit cell sizes fabricated using LPBF

indicates enhanced heat dissipation efficiency, likely attributed to improved surface interaction with the airflow, facilitating more effective thermal management.

In Fig. 9, the Lidinoid heat sink exhibits a well-distributed temperature profile, with peak temperatures reaching 103.58 °C. The temperature contours indicate that the Lidinoid design efficiently facilitates heat dissipation from

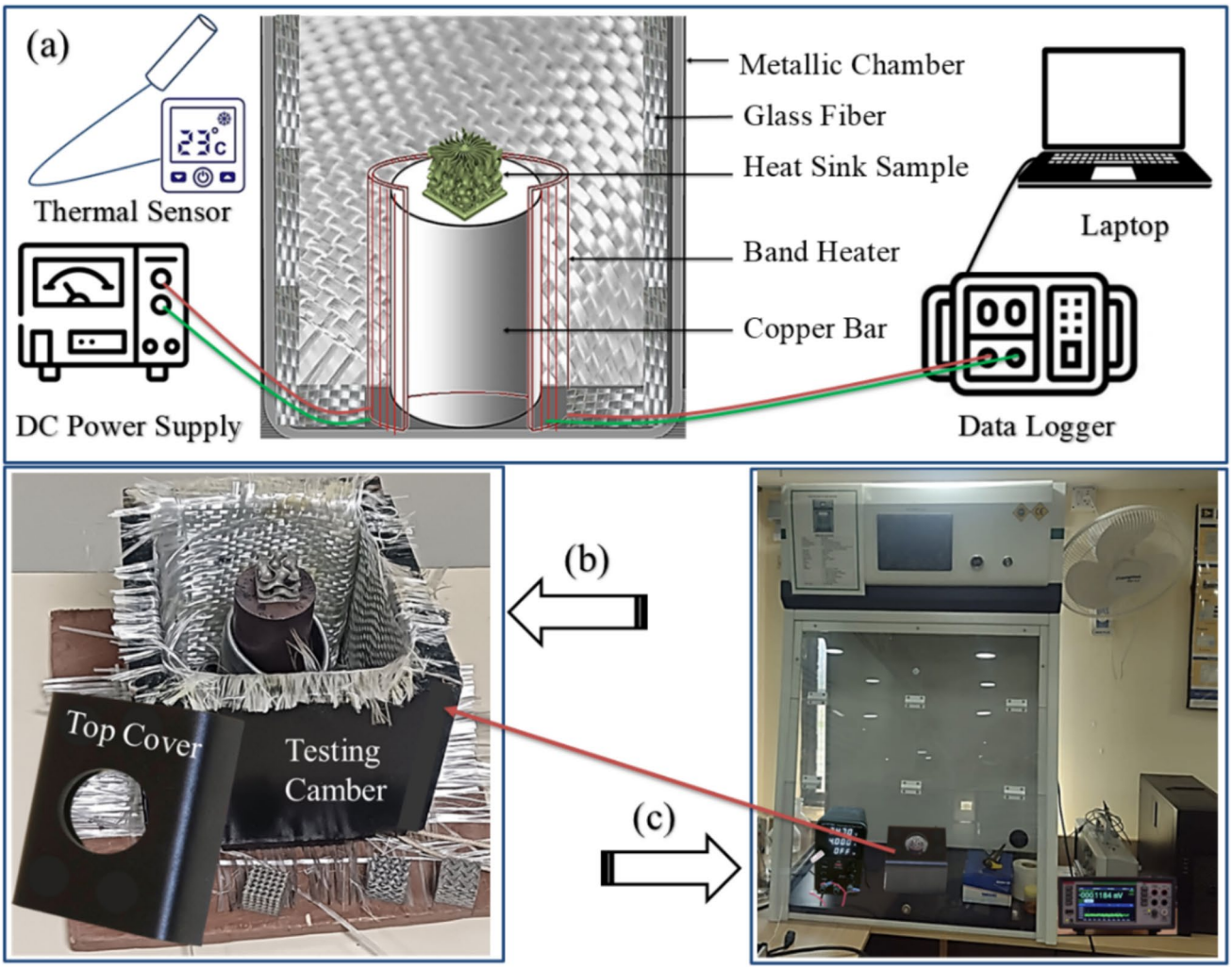

Fig. 6 Schematic of the experimental setup: **a** inner section of the testing chamber, **b** real setup image, and **c** full testing facility to avoid heat losses

the source, ensuring more uniform thermal distribution and maintaining lower average temperatures across the structure.

In addition, (Fig. 9) the Schwarz heat sink exhibits a pronounced thermal gradient, with temperatures ranging from a maximum of 103.58 °C near the heat source to a minimum of approximately 93.7 °C at the distal end. This substantial temperature differential suggests inefficient thermal distribution, indicating the heat sink's limited capacity to effectively dissipate heat across its surface.

Furthermore, Fig. 9 vividly illustrates the pronounced thermal gradient in the conventional heat sink, with temperatures peaking at 102.62 °C near the heat source and dropping to approximately 93.73 °C at the far end. This stark contrast underscores the heat sink's inefficiency in distributing heat evenly, revealing its limitations in thermal management (Figs. 10, 11).

From Table 3, it is found that the temperature gradient is maximum for the diamond (UC10), gyroid (UC5), gyroid (UC10), and split-p (UC10) heat sinks as it covers more area. Therefore, these compact heat sinks have the highest heat transfer. The split-p heat sink with a unit cell size of 10 mm achieves a maximum surface area of 3620 mm^2, offering significantly enhanced thermal performance relative to pin–fin sinks. All TPMS-based heat sinks demonstrate superior heat dissipation characteristics relative to traditional designs. Gyroid, diamond, and split-p heat sinks enable faster cooling through optimized geometry and thermal flow channels. While the periodic variations of the diamond and gyroid structures exhibit commendable thermal performance, they show slightly reduced efficiency compared to their original counterparts. The temperature gradient of diamond lattice heat sinks is 27–35% higher than that of pin

fin heat sinks, while gyroid, split-P, and Schwarz heat sinks exhibit increases of 35%, 44%, and 11%, respectively.

For the temperature versus time analysis of the lattice heat sinks with a unit cell size of 5, the temperature initially increased gradually. At 106 s of heating, the temperature of the pin fin heat sink reached 93 °C, while the Schwarz and Gyroid lattice heat sinks exceeded 100 °C, reaching their peak temperatures. The remaining lattice heat sinks

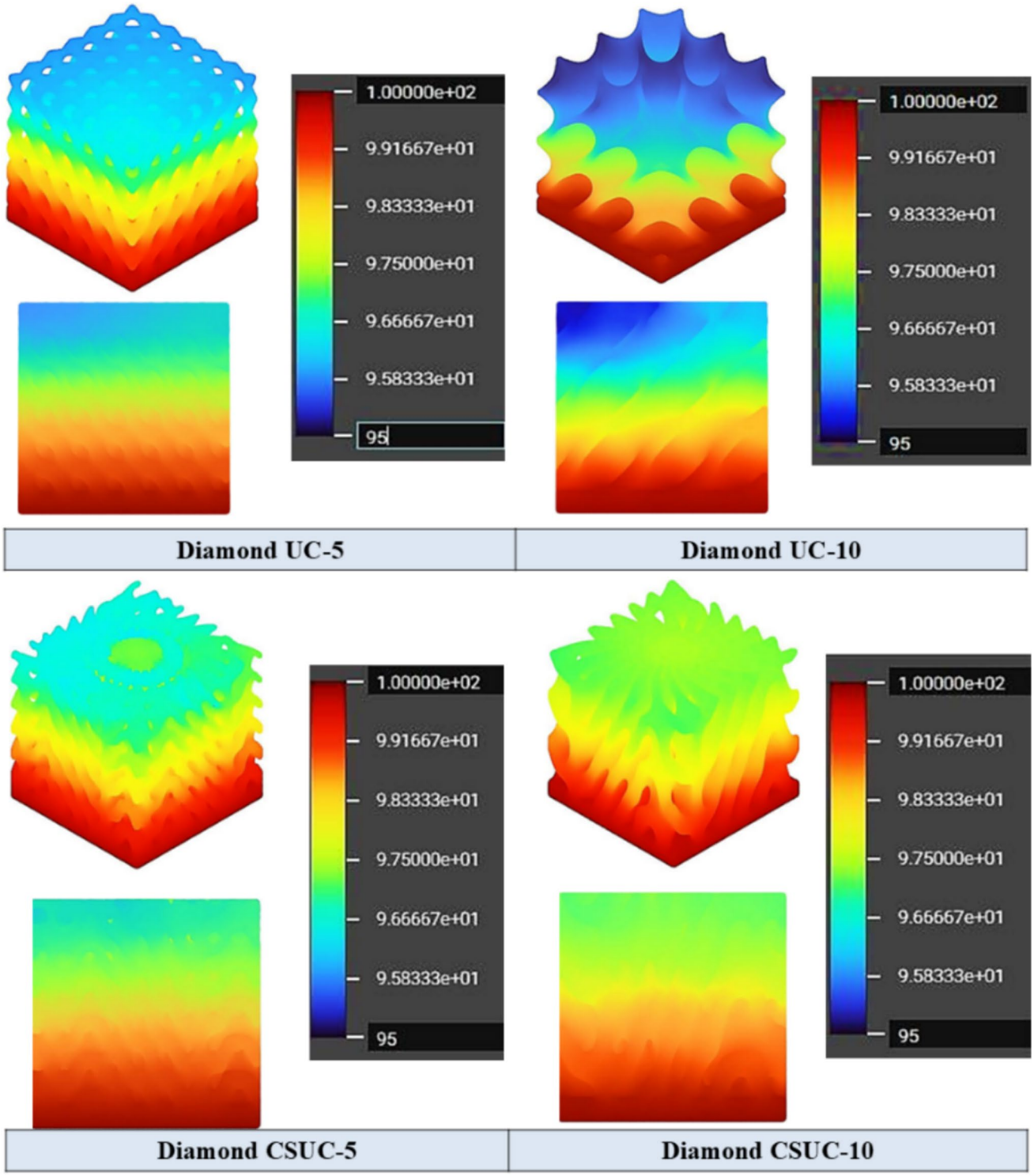

Fig. 7 Temperature contours for the diamond heat sinks (3D and front view)

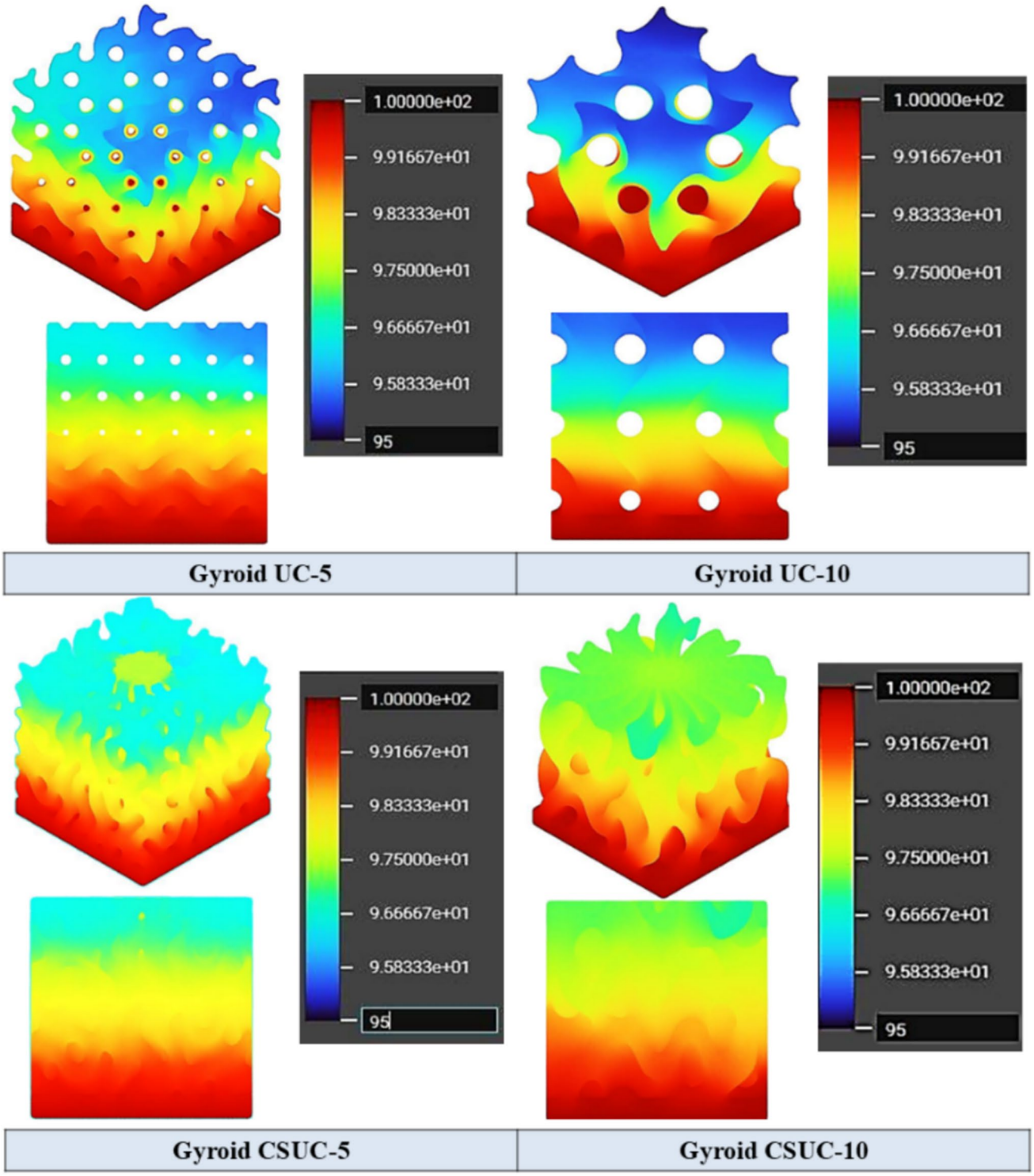

Fig. 8 Temperature contours for gyroid heat sinks (3D and front view)

outperformed the conventional pin fin heat sink, demonstrating superior thermal performance.

3.1 Temperature distribution analysis of heat sinks

The temperature distribution within the heat sink was observed at three key points: the left corner, center, and

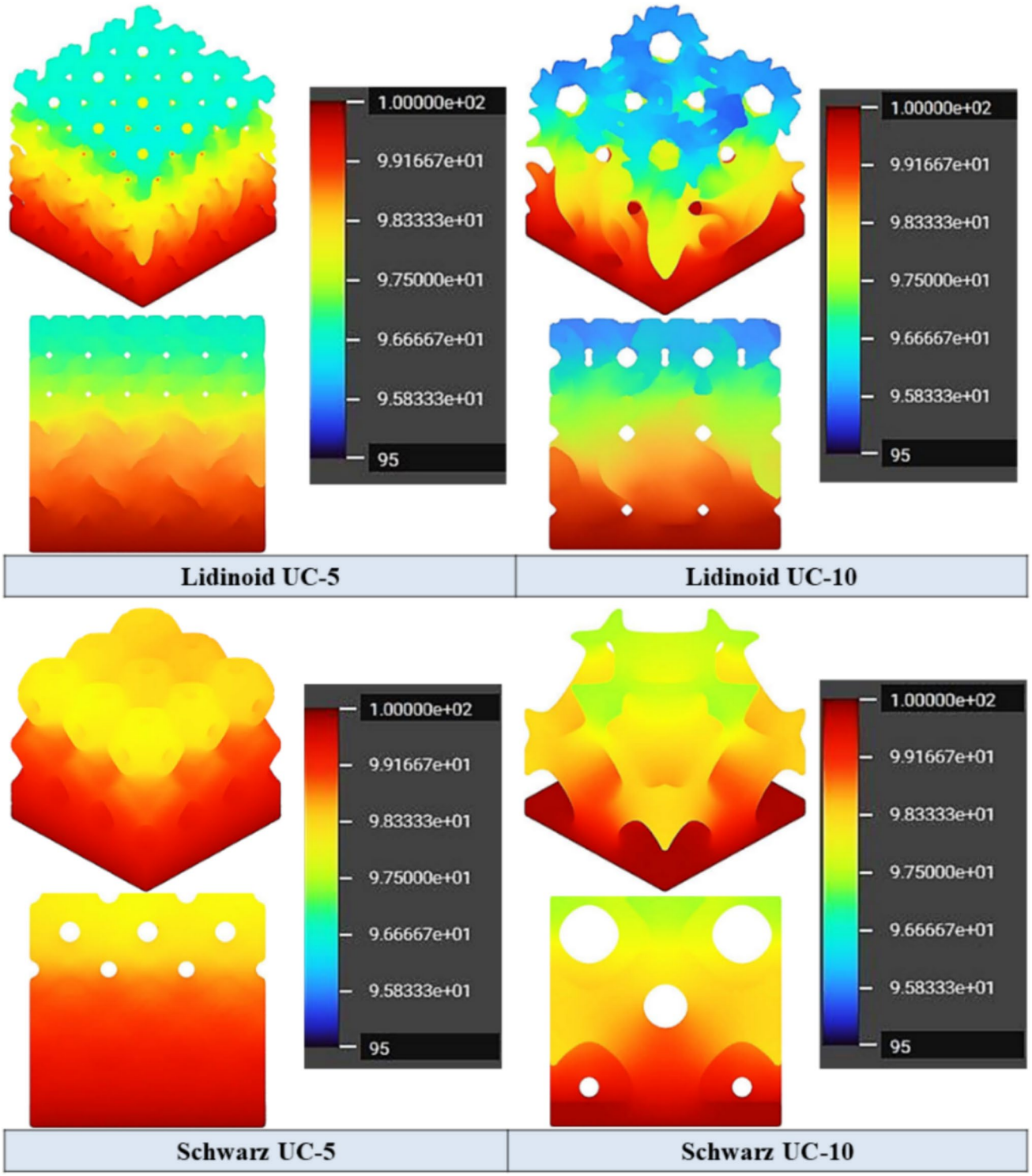

Fig. 9 Temperature contours for lidinoid and Schwarz heat sinks (3D and front view)

right corner, as illustrated in Fig. 12. The selected temperatures for analysis are 40, 60, 80, and 100 °C. Due to the band heater wrapped around the copper cylinder, the outer surface of the heat sink heats up first, followed by the center. Consequently, the left and right portions of the heat sink experience higher temperatures earlier than the center. In lattice heat sinks, the temperature gradient around the center location and the left corner usually falls between 2

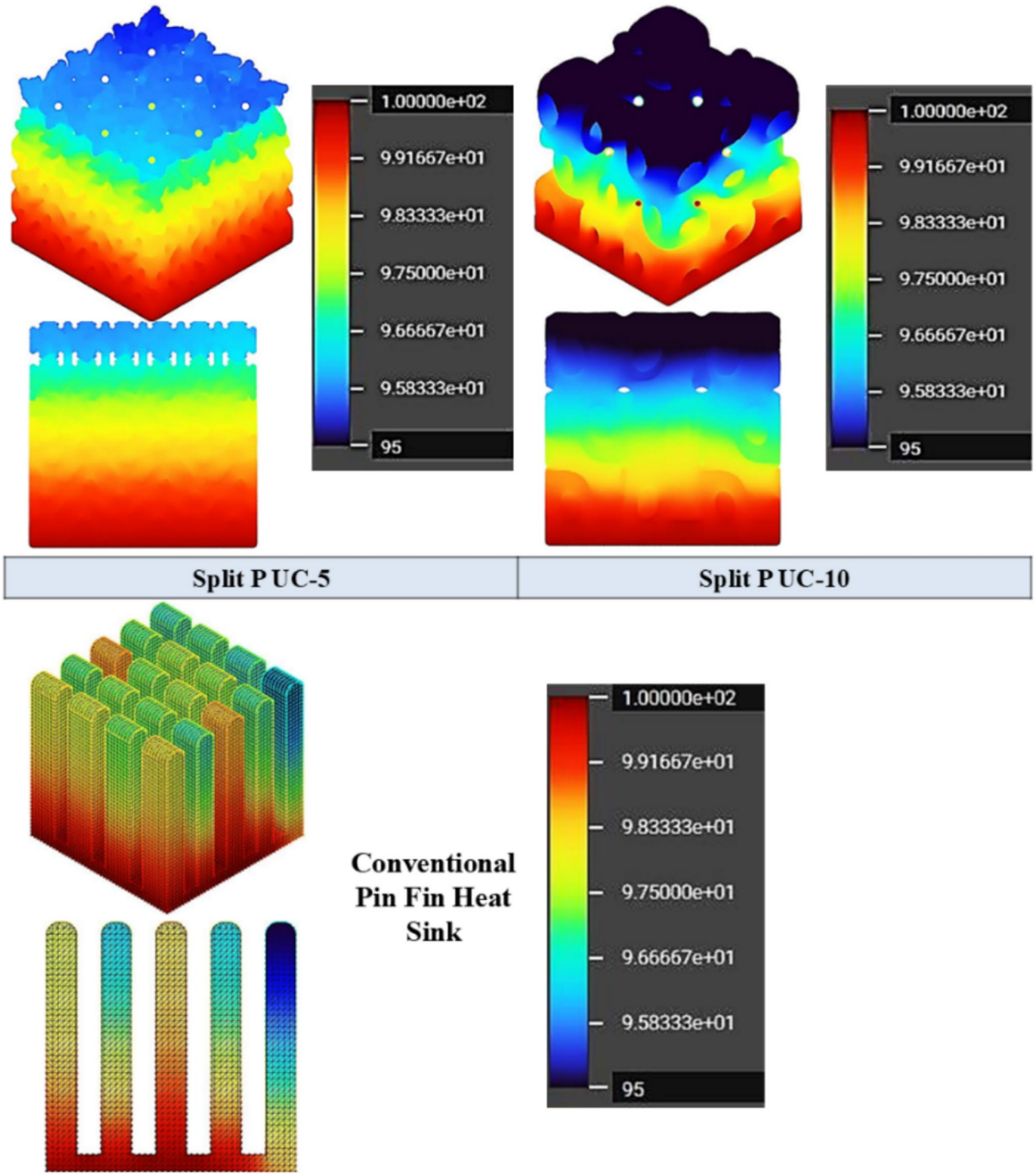

Fig. 10 Temperature contours for split-p and conventional pin fin heat sinks (3D and front view)

and 2.5 °C. Lattice heat sinks exhibit a consistent thermal distribution across the measurement points, whereas conventional heat sinks display more uneven temperature profiles. In pin–fin heat sinks, the thermal distribution varies significantly between individual fins. This continuous and uniform heat distribution observed in lattice heat sinks can be attributed to the interconnected pore network structure inherent in the Triply Periodic Minimal Surface (TPMS) lattices, which facilitates more efficient and homogeneous heat conduction.

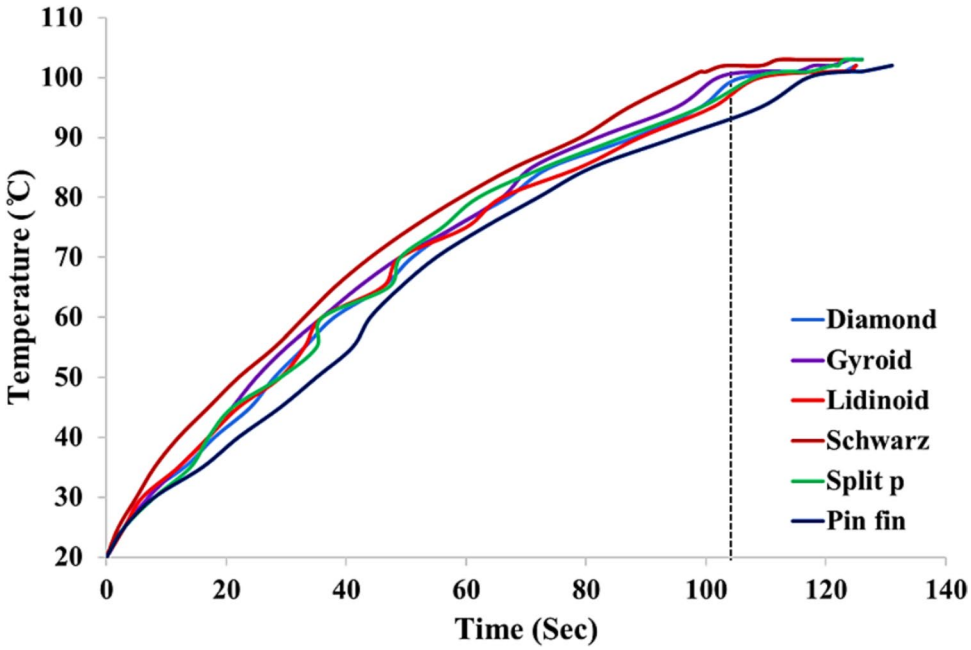

Fig. 11 Time-dependent temperature variation behavior of selected heat sinks

Table 3 Simulation outcomes for various types of TPMS heat sinks

Type of lattice structure	Peak temperature (°C)	Lower temperature (°C)	Temperature difference (°C)
Diamond (UC5)	103.58	92.22	11.37
Diamond (UC10)	103.58	91.54	12.05
Diamond (CS-5)	103.58	91.77	11.82
Diamond (CS-10)	103.58	93.43	10.16
Gyroid (UC5)	103.58	91.54	12.05
Gyroid (UC10)	103.58	91.54	12.05
Gyroid (CS-5)	103.58	92.55	11.04
Gyroid (CS-10)	103.58	93.18	10.41
Lidinoid (UC5)	103.58	92.89	10.69
Lidinoid (UC10)	103.58	91.97	11.62
Split p (UC5)	103.58	91.67	11.92
Split p (UC10)	103.58	90.73	12.86
Schwarz p (UC5)	103.58	93.72	9.87
Schwarz p (UC10)	103.58	93.72	9.87
Conventional pin fin	102.62	93.73	8.89

This study conducts a steady-state thermal characterization of compact TPMS lattice heat sinks with various configurations. The temperature distribution across different heat sink types is illustrated in Fig. 13. The gyroid heat sink exhibited a maximum temperature of 96 °C at an input power of 30 W, which was 11% lower than that of the conventional heat sink. This reduction in temperature can be attributed to the gyroid heat sink's increased surface area and higher geometric complexity compared to other heat sink configurations, which enhance heat dissipation. Furthermore, at an input power of 10 W, the maximum temperatures recorded for the various heat sink designs were as follows: gyroid (65.5 °C), diamond (68.4 °C), lidinoid (72.6 °C), split-p (71.48 °C), Schwarz (75.4 °C), and pin–fin (76.4 °C).

Three observation spots were chosen for additional examination of the heat sink samples following specific simulation findings; two of these points were located within the same plane Fig. 14. Standout differences of all five specimens are the variations in top-to-bottom thermal gradients and heat flow pattern. Temperatures at these three observation spots stabilized after 110 s; the simulation's stabilization period was marginally quicker than the experimental data because of the interstitial radiation structure. Point 1 exhibited a higher temperature than Point 2 for the gyroid lattice heat sink in the same plane. This can be attributed to the outer struts transferring more heat, allowing Point 2 to reach a stable temperature more rapidly. Point 3 at the model's top reached ~ 91 °C, demonstrating heat dissipation via radiation and conduction. In this context, heat conduction occurs within the solid structure, primarily along the direction of the struts and channels. Additionally, heat radiation is generated within the circular holes, thereby enhancing the overall rate of heat dissipation. The temperature increase was most rapid at 21 s, compared to the subsequent 80 s. During the first 21 s, heat transfer occurred predominantly through conduction via the base plate. After 22 s, the heat flow began to penetrate the porous structure, and heat radiation contributed to enhanced heat dissipation. Ultimately, the majority of the heat was radiated into the voids, with only a small portion reaching the floor. The TPMS lattice heat

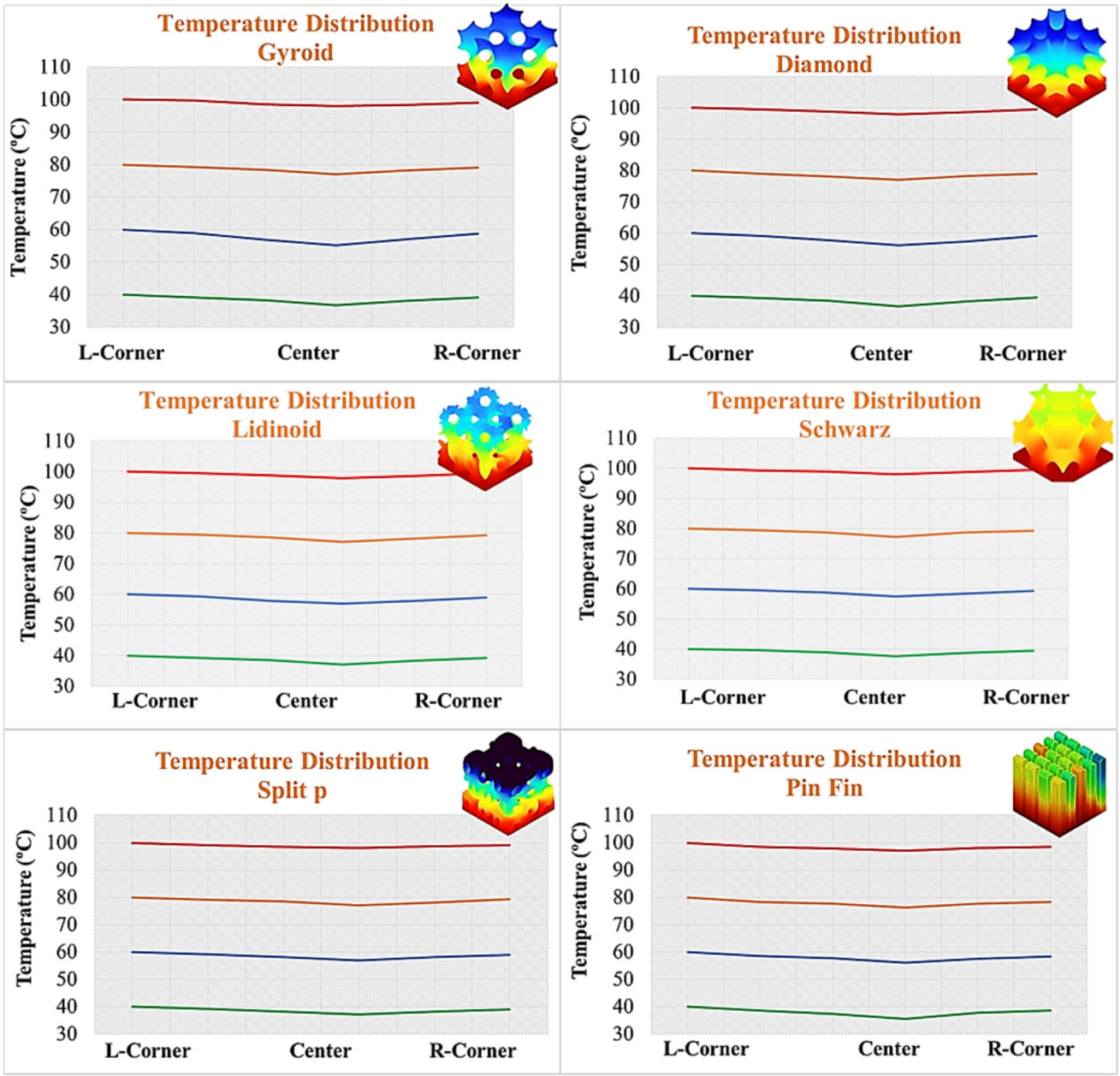

Fig. 12 Heat distribution across the three key points of the heat sink

sinks demonstrated effective thermal insulation throughout the process.

The superior thermal performance of TPMS-based heat sinks can be attributed to three key geometric attributes: connectivity, surface curvature, and porosity distribution. High connectivity ensures multiple, uninterrupted heat conduction pathways from the base plate to the fluid interface, reducing localized thermal bottlenecks. The continuous surface curvature characteristic of TPMS minimizes sharp corners and dead zones, allowing for smoother fluid flow and more uniform boundary layer development. This geometry also facilitates even heat spreading, thereby reducing thermal gradients. The uniform porosity distribution ensures balanced flow resistance and a homogeneous velocity field, which not only promotes consistent cooling throughout the lattice but also prevents local overheating. Together, these features enhance both conduction through the solid lattice and convection to the surrounding fluid, leading to improved overall heat dissipation compared to classical pin–fin or plate–fin designs.

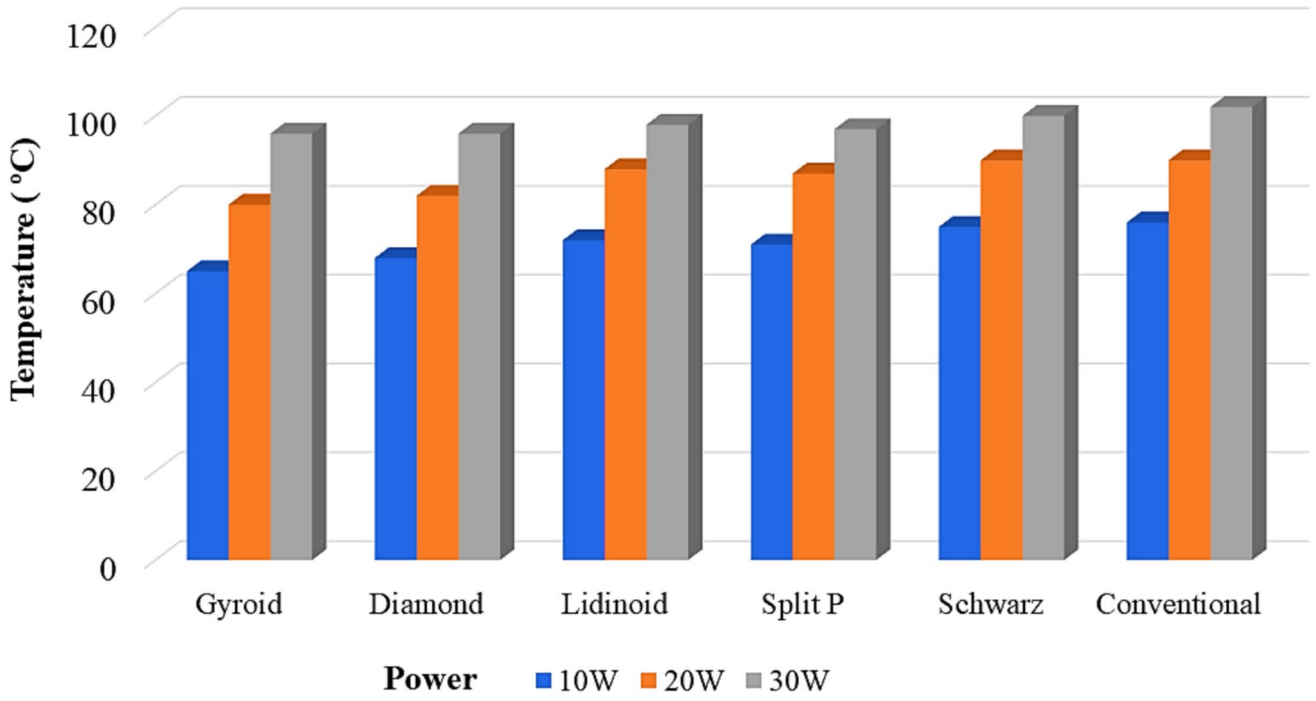

Fig. 13 Effect of input power on temperature scale of heat sinks

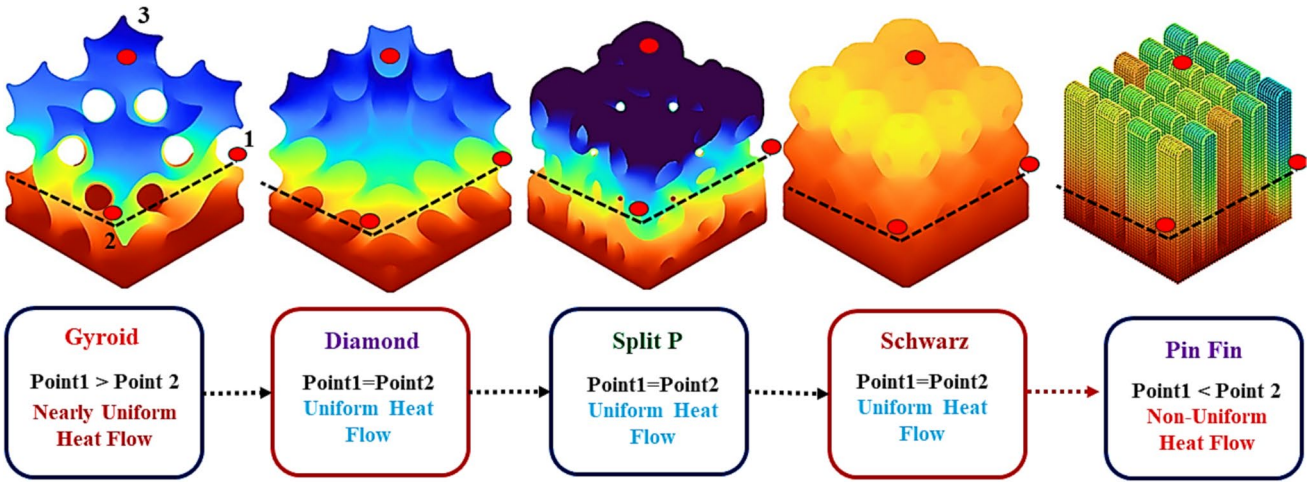

Fig. 14 Heat flow pattern in lattice and conventional heat sinks

4 Conclusion

In this study, a novel heat sink based on TPMS structures was analyzed through thermal simulations and experimental testing. The simulations were performed under various thermal loads to evaluate the influence of cell size, porosity, and periodicity on heat transfer enhancement. A customized testing system was employed to validate heat flow and measure temperature gradients from bottom to top, along with temperature variations at different locations of L-PBF printed heat sinks.

The results clearly indicate that the surface temperature of the heat sink decreases for lattice heat sinks. This temperature reduction is attributed to the increased surface area provided by the new design. This indicates that a greater amount of heat is conducted to the lattice heat sinks, which subsequently dissipate it into the surrounding environment through convection. The results indicate a more uniform temperature distribution in the TPMS lattice heat sinks,

attributed to their intricate, tortuous internal structure, in contrast to conventional heat sinks. The heat transfer in lattice heat sinks is 25–45% higher than conventional heat sinks.

As we move toward the future, the varying periodicity lattice heat sinks exhibit moderate performance compared to natural periodic lattice heat sinks but demonstrate a 13% improvement in thermal efficiency over conventional heat sinks. The surface area of additively manufactured (AM) lattice heat sinks fabricated from aluminum is increased by up to 200% compared to conventional heat sink designs. In addition, the findings suggest that additive manufacturing's ability to create complex geometries and compact sizes improves thermal dissipation, identifying TPMS lattice heat sinks (1 mm wall thickness, 15 mm size) as the most efficient for heat transfer.

Further research can explore the different varying periodicity patterns to investigate thermal behavior. In addition, thermal analysis indicates a higher concentration of heat at the base of the lattice heat sinks, attributed to the increased cell thickness and reduced size at the bottom. This structural configuration enhances heat conduction from the source to the samples, improving overall thermal performance.

Future work will focus on the investigation of hybrid material strategies through multi-material LPBF, such as copper–aluminum or graded alloys, to leverage the combined benefits of high thermal conductivity and reduced weight in compact heat sink designs. In parallel, extended design optimization of TPMS- and lattice-based geometries will be pursued using advanced computational tools to further improve thermal performance while ensuring mechanical robustness. Additionally, metal binder jetting will be explored as an alternative manufacturing route to investigate its influence on surface morphology, dimensional accuracy, and overall thermal–structural performance.

Supplementary Information The online version contains supplementary material available at https://doi.org/10.1007/s40964-025-01366-0.

Acknowledgements For the purpose of open access, the author has applied a Creative Commons Attribution (CC BY) license to any Author Accepted Manuscript version arising from this submission. This work is supported by nTopology and we appreciate for providing generic education version software which enabled the advanced computational design and analysis conducted in this research.

Author contributions G.C—original draft, methodology, and results. A.K—formal analysis. A.G—simulation. K.E—supervision. P.B—supervision and review.

Data availability On request, the corresponding authors will provide all information and materials necessary to produce the findings in this study.

Declarations

Conflict of interest The authors declared no conflict of interest.

Ethical approval The authors declare that there is no ethical issue applicable to this article.

Open Access This article is licensed under a Creative Commons Attribution 4.0 International License, which permits use, sharing, adaptation, distribution and reproduction in any medium or format, as long as you give appropriate credit to the original author(s) and the source, provide a link to the Creative Commons licence, and indicate if changes were made. The images or other third party material in this article are included in the article's Creative Commons licence, unless indicated otherwise in a credit line to the material. If material is not included in the article's Creative Commons licence and your intended use is not permitted by statutory regulation or exceeds the permitted use, you will need to obtain permission directly from the copyright holder. To view a copy of this licence, visit http://creativecommons.org/licenses/by/4.0/.

References

1. López-García C, García-López E, Siller H et al (2022) A dimensional assessment of small features and lattice structures manufactured by laser powder bed fusion. Prog Addit Manuf. https://doi.org/10.1007/s40964-022-00263-0
2. Ding J, Qu S, Zhang L et al (2022) Geometric deviation and compensation for thin-walled shell lattice structures fabricated by high precision laser powder bed fusion. Addit Manuf 58:103061
3. McGregor M, Patel S, Zhang K et al (2024) A manufacturability evaluation of complex architectures by laser powder bed fusion additive manufacturing. J Manuf Sci Eng. https://doi.org/10.1115/1.4065315
4. Guillen D, Wahlquist S, Ali A (2024) Critical review of LPBF metal print defects detection: roles of selective sensing technology. Appl Sci 14:6718
5. Sunku Prasad J, Anandalakshmi R, Muthukumar P (2021) Numerical investigation on conventional and PCM heat sinks under constant and variable heat flux conditions. Clean Technol Environ Policy 23:1105–1120. https://doi.org/10.1007/s10098-020-01829-8
6. Chouhan G, Bidare P, Bala Murali G (2024) Triply periodic minimal surface based lattices for acoustic performance. Noise Vib Worldw 55:454–468. https://doi.org/10.1177/09574565241270201
7. Chouhan G, Bala Murali G (2023) Designs, advancements, and applications of three-dimensional printed gyroid structures: a review. Proc Inst Mech Eng Part E J Process Mech Eng. https://doi.org/10.1177/09544089231160030
8. Tang D, Xu S, Yang K et al (2023) Effects of porosity on effective thermal conductivities of thermal insulation SiC sandwich panels with Schoen-gyroid structure. Ceram Int 50:10618–10625. https://doi.org/10.1016/j.ceramint.2023.12.375
9. Günther F, Pilz S, Hirsch F et al (2023) Shape optimization of additively manufactured lattices based on triply periodic minimal surfaces. Addit Manuf 73:103659. https://doi.org/10.1016/j.addma.2023.103659
10. Ormiston S, Srinivas Sundarram S (2024) Fiberglass-reinforced triply periodic minimal surfaces (TPMS) lattice structures for energy absorption applications. Polym Compos 45:523–534. https://doi.org/10.1002/pc.27795
11. Rathore S, Mehta B, Kumar P, Asfer M (2022) Flow characterization in triply-periodic-minimal-surface (TPMS) based porous geometries: part 1 -hydrodynamics. Transp Porous Media. https://doi.org/10.1007/s11242-022-01880-7

12. Chouhan G, Bidare P (2024) Manufacturability of A20X printed lattice heat sinks. Prog Addit Manuf. https://doi.org/10.1007/s40964-024-00923-3
13. Baobaid N, Ali MI, Khan KA, Abu Al-Rub RK (2022) Fluid flow and heat transfer of porous TPMS architected heat sinks in free convection environment. Case Stud Therm Eng 33:101944. https://doi.org/10.1016/J.CSITE.2022.101944
14. Al-Ketan O, Ali M, Khalil M et al (2021) Forced convection computational fluid dynamics analysis of architected and three-dimensional printable heat sinks based on triply periodic minimal surfaces. J Therm Sci Eng Appl. https://doi.org/10.1115/1.4047385
15. Hassan Ali M, Alketan O, Khalil M et al (2020) 3D printed architected heat sinks cooling performance in free and forced convection environments. In: Proceedings of the ASME 2020 Heat Transfer Summer Conference, pp 1–7. https://doi.org/10.1115/HT2020-9067
16. Naranjani B, Roohi E, Ebrahimi A (2021) Thermal and hydraulic performance analysis of a heat sink with corrugated channels and nanofluids. J Therm Anal Calorim 146:2549–2560. https://doi.org/10.1007/s10973-020-10225-9
17. Chang YC (2020) Simulation analysis of heat transfer performance of heat sink with reduced material design. Adv Mech Eng 12:1–7. https://doi.org/10.1177/1687814020921300
18. Saadoon ZH, Ali FH, Hamzah HK et al (2022) Improving the performance of mini-channel heat sink by using wavy channel and different types of nanofluids. Sci Rep. https://doi.org/10.1038/s41598-022-13519-0
19. Xiang J, Deng L, Zhou C et al (2022) Heat transfer performance and structural optimization of a novel micro-channel heat sink. Chin J Mech Eng. https://doi.org/10.1186/s10033-022-00704-5
20. Sushma S, Chandrashekar TK (2021) An experimental investigation on performance of heat transfer using heat sink of different shape for electronic applications. Indian J Sci Technol 14:2789–2801. https://doi.org/10.17485/ijst/v14i35.1179
21. Obaid AJ, Hameed VM (2023) An experimental and numerical comparison study on a heat sink thermal performance with new fin configuration under mixed convective conditions. S Afr J Chem Eng 44:81–88. https://doi.org/10.1016/j.sajce.2023.01.009
22. Qureshi ZA, Elnajjar E, Al-Ketan O et al (2021) Heat transfer performance of a finned metal foam-phase change material (FMF-PCM) system incorporating triply periodic minimal surfaces (TPMS). Int J Heat Mass Transf 170:121001
23. Bharadwaj, B, Singh, P, Mahajan R (2022) Optimal design of additively manufactured metal lattice heat sinks for electronics cooling. In: Proc ASME 2022 Heat Transf Summer Conf collocated with ASME 2022 16th Int Conf Energy Sustain ASME 2022 Heat Transf Summer Conf Philadelphia, Pennsylvania, USA, July 11–13, 2022, V001T16A002 A 11–13. https://doi.org/10.1115/HT2022-85400
24. Vaissier B, Pernot JP, Chougrani L, Véron P (2019) Parametric design of graded truss lattice structures for enhanced thermal dissipation. CAD Comput Aided Des 115:1–12. https://doi.org/10.1016/j.cad.2019.05.022
25. Niranjan RS, Singh O, Ramkumar J (2022) Numerical study on thermal analysis of square micro pin fins under forced convection. Heat Mass Transf und Stoffuebertragung 58:263–281. https://doi.org/10.1007/s00231-021-03105-x
26. Gaikwad A, Sathe A, Sanap S (2023) A design approach for thermal enhancement in heat sinks using different types of fins: a review. Front Therm Eng 2:1–13. https://doi.org/10.3389/fther.2022.980985
27. Liu J, Hu L, Lui K-W et al (2025) Design and characterization of breathable 3D printed textiles with flexible lattice structures. J Manuf Process 141:48–58
28. Lin Y, Zhu L, Chen Y et al (2024) An enhanced spatial extrusion method to manufacture large-scale thermoplastic lattice structures. Addit Manuf 92:104393
29. Mora S, Pugno NM, Misseroni D (2022) 3D printed architected lattice structures by material jetting. Mater Today 59:107–132. https://doi.org/10.1016/J.MATTOD.2022.05.008
30. Cho J, Kim E, Kim JH et al (2025) Enhancement of energy absorption capability of 3D printed Ti–6Al–4V BCC lattice structures by adding auxiliary struts. Materials (Basel). https://doi.org/10.3390/ma18040732
31. Jafari D, Wits WW (2018) The utilization of selective laser melting technology on heat transfer devices for thermal energy conversion applications: a review. Renew Sustain Energy Rev 91:420–442. https://doi.org/10.1016/j.rser.2018.03.109
32. Wong KK, Ho JY, Leong KC, Wong TN (2016) Fabrication of heat sinks by selective laser melting for convective heat transfer applications. Virtual Phys Prototyp 11:159–165. https://doi.org/10.1080/17452759.2016.1211849
33. Deng Y, Fu L, Liu Y et al (2022) Investigation on heat transfer characteristics of rectangular channels with internal rough surface naturally formed by selective laser melting three-dimensional printing. J Fluids Eng. https://doi.org/10.1115/1.4054862
34. Constantin L, Wu Z, Li N et al (2020) Laser 3D printing of complex copper structures. Addit Manuf. https://doi.org/10.1016/j.addma.2020.101268
35. Qureshi ZA, Addin Burhan Al-Omari S, Elnajjar E et al (2022) On the effect of porosity and functional grading of 3D printable triply periodic minimal surface (TPMS) based architected lattices embedded with a phase change material. Int J Heat Mass Transf 183:122111
36. Jadhav SV, Pawar PM, Wangikar SS et al (2020) Thermal management materials for advanced heat sinks used in modern microelectronics. IOP Conf Ser Mater Sci Eng. https://doi.org/10.1088/1757-899X/814/1/012044
37. Forde J (2013) A20X—high strength, elevated temperature aluminium casting alloy. In: Conf Aeromat 24 Conf Expo Am Soc Met
38. Ghasri-Khouzani M, Karimialavijeh H, Pröbstle M et al (2023) Processability and characterization of A20X aluminum alloy fabricated by laser powder bed fusion. Mater Today Commun 35:105555

Publisher's Note Springer Nature remains neutral with regard to jurisdictional claims in published maps and institutional affiliations.